JACS
JOURNAL OF THE AMERICAN CHEMICAL SOCIETY
Article
pubs.acs.org/JACS
Terms of Use

Interactions of Protein Kinase C-α C1A and C1B Domains with Membranes: A Combined Computational and Experimental Study

Jianing Li,[†] Brian P. Ziemba,[‡] Joseph J. Falke,[‡] and Gregory A. Voth*,[†]

[†]Department of Chemistry, Institute for Biophysical Dynamics, James Franck Institute and Computation Institute, The University of Chicago, 5735 South Ellis Avenue, Chicago, Illinois 60637, United States

[‡]Department of Chemistry and Biochemistry and the Molecular Biophysics Program, University of Colorado at Boulder, Boulder, Colorado 80309, United States

Supporting Information

ABSTRACT: Protein kinase C-α (PKCα) has been studied widely as a paradigm for conventional PKCs, with two C1 domains (C1A and C1B) being important for the regulation and function of the kinase. However, it is challenging to explore these domains in membrane-bound environments with either simulations or experiments alone. In this work, we have combined modeling, simulations, and experiments to understand the molecular basis of the PKCα C1A and C1B domain interactions with membranes. Our atomistic simulations of the PKCα C1 domains reveal the dynamic interactions of the proteins with anionic lipids, as well as the conserved hydrogen bonds and the distinct nonpolar contacts formed with lipid activators. Corroborating evidence is obtained from additional simulations and experiments in terms of lipid binding and protein diffusion. Overall, our study, for the first time, explains with atomistic detail how the PKCα C1A and C1B domains interact differently with various lipids. On the molecular level, the information provided by our study helps to shed light on PKCα regulation and activation mechanism. The combined computational/experimental approach demonstrated in this work is anticipated to enable further studies to explore the roles of C1 domains in many signaling proteins and to better understand their molecular mechanisms in normal cellular function and disease development.

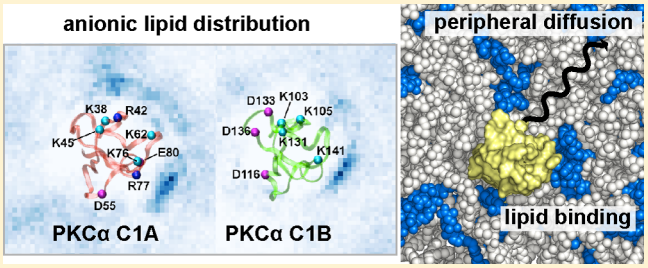

INTRODUCTION

When recruited from the cytosol to the membrane, many signaling proteins are activated in response to binding lipid activators with their membrane-binding domains.[1−3] As a paradigmatic class of membrane-binding domains, C1 domains play vital regulatory roles in a large number of signaling proteins such as protein kinase C (PKC), protein kinase D (PKD), diacylglycerol kinase (DAGK), and chimerin.[4−8] Each C1 domain contains about 5 short interlacing strands and a C-terminal helix, which are organized around two integral Zn^{2+} ions (Figure 1A). In the sequences of C1 domains, a characteristic motif, $HX_{10-12}CX_2CX_{9-15}CX_2CX_4HX_{2-4}CX_{6-8}C$, has been identified, where H and C represent the conserved histidine and cysteine residues to coordinate the Zn^{2+} ions, and X can be any amino acid.[4,9,10] It is believed that the hydrophobic half of a C1 domain, comprised primarily of the β12 and β34 loops, penetrates into the hydrocarbon core of the membrane,[2,11,12] while the hydrophilic half with Zn^{2+} ions and several ionic residues on the surface is exposed to the cytosol (Figure 1B−D).

Despite high sequence homology and structural similarities,[4,9] the C1 domains of different proteins exhibit wide-ranging binding affinities to anionic lipid coactivators like 1,2-*sn*-phosphatidyl-L-serine (PS), as well as to neutral lipid activators like 1,2-*sn*-diacylglycerol (DAG) and phorbol-12-myristate-13-acetate (PMA). In particular, many typical C1 domains of PKCs bind DAG or PMA preferentially, while others have comparable affinities to both activators.[13] There also exist atypical C1 domains that bind neither DAG nor PMA.[4] These differences in binding affinities and preferences are challenging to explain on the basis of the currently available, limited structural data alone. At present merely 13 distinct C1 domains have been deposited to the Protein Data Bank (PDB), and thus there is no three-dimensional (3D) information for over 90% of the C1 domains with known sequences.[1] Furthermore, only a single structure in complex with any lipid activator has been solved with X-ray crystallography.[11] As a result, key structural details of C1 domains, for instance, interactions with anionic lipids and DAG as well as the protein orientation and degree of membrane penetration, have not been elucidated fully. Given the experimental challenges of studying C1 domains in membrane-bound environments,[2,14,15] computer modeling and atomistic simulations provide a useful means to explore the detailed interactions and conformations involved in membrane binding and recognition of lipid activators, which will likely enhance our understanding of the

Received: May 28, 2014
Published: July 30, 2014

   dx.doi.org/10.1021/ja505369r | J. Am. Chem. Soc. 2014, 136, 11757−11766

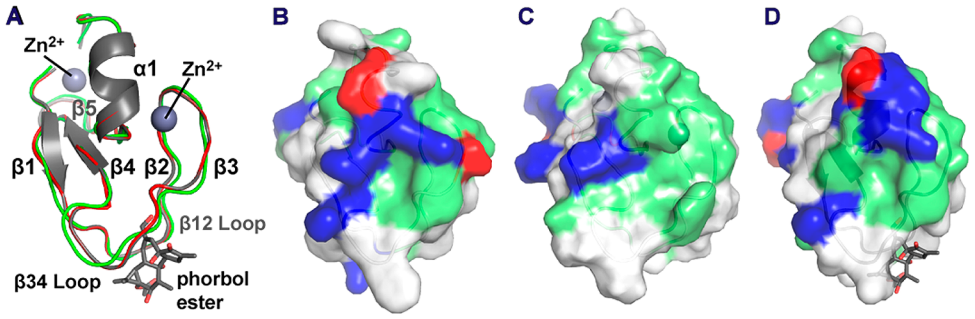

Figure 1. (A) Superimposed structures of the PKCα C1A domain (a homology model; red), the PKCα C1B domain (PDB code: 2ELI; green), and the ligand-bound PKCδ C1B domain (PDB code: 1PTR; gray). The C_α RMSD is 0.1 Å between the PKCα C1A model and the PKCδ C1B structure, and 0.7 Å between the PKCα and PKCδ C1B structures. Surface representations of (B) the PKCα C1A domain, (C) the PKCα C1A domain, and (D) the ligand-bound PKCδ C1B domain are also shown. In panels B, C, and D, basic, acidic, and neutral polar residues are shown in blue, red, and green, respectively.

C1 domain roles for the function and regulation of signaling proteins.

A combined computational and experimental study is presented in this work with the aim of investigating the interactions between the C1 domains in the PKC alpha isoform (PKCα) and their lipid partners (PS, DAG, and PMA). Implicated in a large number of human diseases[16,17] including cancers,[18,19] cardiovascular diseases,[20,21] diabetes and complications,[22,23] as well as bipolar disorder,[24,25] PKCα is widely studied as a model for conventional PKCs (cPKCs: α, βI, βII, and γ isoforms) for understanding how C1 domains regulate signaling proteins.[9] Similar to other cPKCs, PKCα possesses two tandem C1 domains,[26] namely, C1A and C1B, in addition to a C2 targeting domain and a C-terminal kinase domain.[9] The evidence shows that a mature PKCα in its compact inactive state is activated via sequential binding of individual domains to the plasma membrane surface.[27−30] At first, calcium triggers C2 domain binding to anionic lipids and the entire PKCα protein is directed to the membrane. Dissociating from the kinase domain, the inhibitory C1A and C1B domains are then recruited to the membrane to bind lipid coactivators (such as PS) and activators (such as DAG and PMA). This process results in an activated PKCα, which catalyzes the phosphorylation of substrate proteins.[9]

Significant recent progress[29,31] highlights the importance of the two C1 domains in the activation mechanism, and the need for further computational and experimental efforts are required to better understand the membrane interactions of these domains. A growing body of experimental evidence suggests that the two C1 domains in cPKCs are not equivalent, but the molecular basis for this nonequivalence is only partly understood.[10] For example, although both C1 domains are thought to interact with membranes, some evidence suggests that only one of the two cPKC C1 domains can bind to a lipid activator.[32] Other results suggest that, in the case of PKCα, both domains bind to activators[28,29] yet with opposite affinities.[13,33] It is generally believed that the PKCα C1A domain has a higher affinity for DAG than the C1B domain, while the latter has a higher affinity for PMA.[14,33,34] Regarding mutations of equivalent or ionic residues, more pronounced impacts appeared in the C1A domain than in the C1B domain on PKCα membrane binding and activation.[35−37] Lastly, in the cPKC activation mechanism, recent work indicate that C1A stabilizes the predominant activation intermediate by binding first to the membrane, even in the absence of activating lipid.[29] In this model, recruitment of C1B to the membrane by activating lipid is the key step in kinase activation.[29,38] To further elucidate the roles of the C1A and C1B domains in PKCα activation, it is essential to understand their detailed molecular interactions with membranes. Therefore, we have combined computational and experimental approaches in this work to characterize the interactions of the PKCα C1A and C1B domains with various lipids in different membrane environments.

Because of the shortage of experimentally determined structures and membrane-docking geometries of the cPKC C1 domains, it is a challenge to employ computer simulations to compare the two C1 domains from the same cPKC in membrane-bound environments. While most prior docking and simulation studies focused on the C1B domains of PKCα and PKCδ in solution,[37,39−41] only the PKCγ C1B domain has been simulated in a lipid bilayer.[42] To the best of our knowledge, a comparative study of both C1A and C1B domains in membranes has never been reported. Given our recent computational and experimental progress in PKCα research,[12,29,43] it has now become viable to employ a combined approach to reveal and compare details of the two PKCα C1 domains in membranes. As presented in this work, we have built the atomistic PKCα C1A and C1B models in different membrane-bound environments and performed a systematic investigation combining findings from simulations and experiments. Synergy between simulations and experiments enabled us to access structural and dynamic details of the C1 domain-lipid complexes at various spatial and temporal scales. Our combined study aimed to help understand the atomistic details of the PKCα C1 domain-lipid interactions that have not been fully described before, and to provide valuable new insight about the roles of the C1 domains in PKCα regulation and activation.

RESULTS AND DISCUSSION

PKCα C1 Domains in the PC:PS Membrane. Since PS lipid is an essential coactivator for cPKC binding to membranes,[44] we first performed atomistic molecular dynamics (MD) simulations with an individual C1A or C1B domain in the 3:1 PC:PS membrane, to examine the interactions between the proteins and PS. In both cases, the C_α RMSDs rise over the first 20−26 ns, and then stabilize between 1.5 and 2.0 Å for the rest of the simulations, which demonstrates structural stability of our membrane-bound protein models. The major deviation from the reference, the PKCα C1B structure in solution (PDB code: 2ELI), is the increased separation between the β12 and

dx.doi.org/10.1021/ja505369r | J. Am. Chem. Soc. 2014, 136, 11757−11766

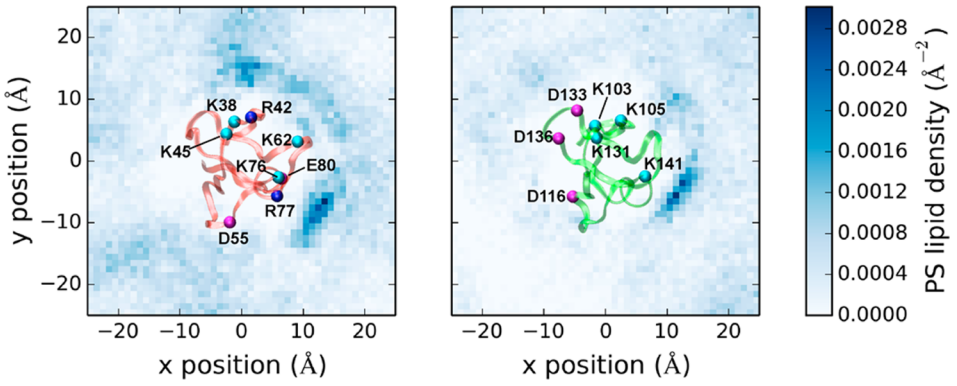

Figure 2. PS headgroup density maps of the PKCα C1A domain (left panel) and the C1B domain (right panel). The blue contours show the surface density of PS lipid head groups in the lower membrane leaflet based on the 300 ns simulations. With a viewpoint from the bottom of the simulation box, the protein backbones are shown as ribbons and the C_α atoms of ionic residues as beads.

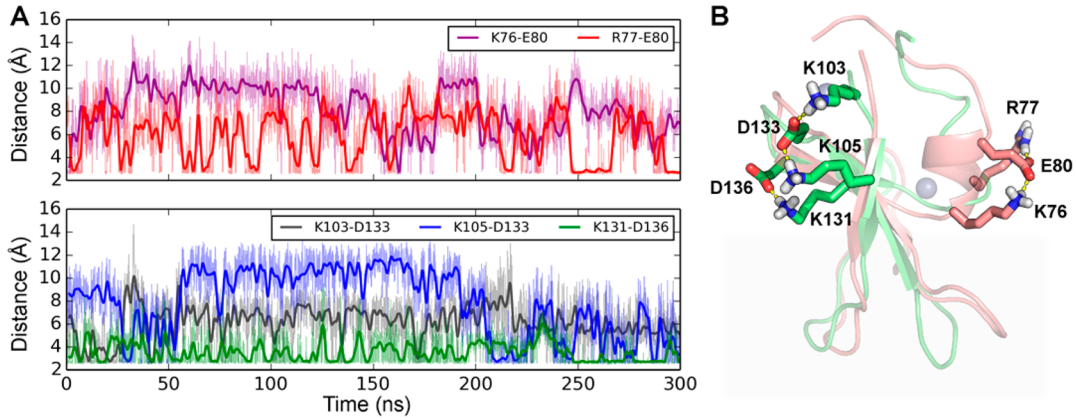

Figure 3. (A) Time evolution of intramolecular salt bridges in the 300 ns simulations of the PKCα C1A (top panel) and C1B domains (bottom panel) in the PC:PS membrane. The raw and smoothed data are illustrated as thin and thick lines, respectively. (B) Structural representations of the salt-bridge network at 290 ns of the apo C1A simulation (pink backbone) and at 293 ns of the apo C1B simulation (green backbone). Zn^{2+} ions are shown as silver spheres. To illustrate the membrane insertion, a shadow box is used to indicate the membrane as a guide for the eyes. The ligand binding sites are open in both conformations.

β34 loop tips, defined as the C_α distance between Q46 and F60 in the C1A domain or S111 and L125 in the C1B domain.[37] The increased loop separation leads to opening of the activator-binding groove, albeit to different extents in these two domains (see Supporting Information (SI), Figure S1A). The C1B domain shows a slight increase in the loop-tip distance from 11.5 Å to an average value of 12.2 Å, with a broad distribution from 9 to 16 Å. The conformations sampled in our simulations agree well with the open-loop conformations (~12.5 Å) that were observed in an earlier simulation study with the same C1B domain.[37]

Compared to the C1B domain, the C1A domain appears to possess a wider activator-binding groove, presumably due to the presence of more flexible β12 and β34 loops. The loop-tip distance is generally 2−3 Å longer, compared to the corresponding distance of the C1B domain, with a distribution centered at 15.3 Å (Figure S1A (SI)). Overall, in the absence of activators, the increased separation of the loop tips as well as the resulting open activator-binding groove in the PKCα C1 domains, suggests that interactions with PC:PS membrane stabilizes the open-loop conformations and may facilitate activator interactions.

While association with the PC:PS membrane induces conformational changes of the C1 domains, the proteins also shape the local PS distribution. The lateral distributions of the PS head groups are shown in Figure 2, which reveals the similarities and differences between the C1A and C1B domains in terms of interactions with the PS lipids. On one hand, given no detectable density in the protein-occupied regions, the PS head groups only associate at the periphery of the C1 domains, remaining excluded from the activator-binding grooves in both cases. It is likely that, in their roles as coactivators, anionic lipids such as PS hardly interfere with activator binding. On the other hand, as shown by the distinct high-density regions, the PS lipids interact with the two C1 domains at very different sites. The PKCα C1A domain has a number of basic residues (i.e., R42, K45, K62, K76 and R77) on one face, corresponding to a semiannular region with a high PS density. The other face adjacent to the low-density region is made up mainly of several aromatic residues (i.e., F49, F56, W58, and F72) and an acidic residue D55. In contrast, the PKCα C1B domain has high PS density only near two basic residues, K105 and K141. Most of the membrane region around the C1B domain shows a much lower PS density than observed around the C1A domain periphery. This phenomenon cannot be attributed simply to fewer basic and more acidic residues in the PKCα C1B domain than in the C1A domain. Our further analysis of ionic residues reveals a stable salt-bridge network in the C1B domain, which leads to the following explanation: Two sets of charged residues that are consistently interacting, K103-D133-K105 and K131-

dx.doi.org/10.1021/ja505369r | J. Am. Chem. Soc. 2014, 136, 11757−11766

D136, form a salt-bridge network in the C1B domain (Figure 3). Such a salt-bridge network (i) reduces the number of free basic residues and (ii) weakens the protein-PS contacts, so that the C1B domain is less able to attract PS lipids. By contrast, a similar network is not observed in the case of the C1A domain: There are varying electrostatic contacts between residues K76-E80-R77, but the basic residues are still allowed to bind PS lipids (Figures 3 and 4). Therefore, our simulations suggest that

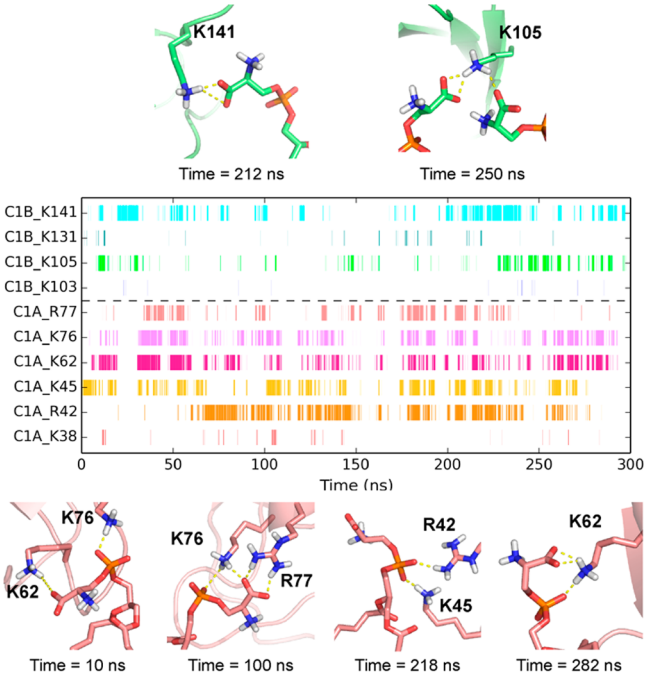

Figure 4. Eventplot of the key basic residues that associate with the PS lipids. Each line in the eventplot represents the occurrence of the basic residue with a bound PS lipid. Simulation snapshots at various time intervals are taken to show the multivalent binding.

distinct electrostatic detailed interactions are responsible for the observed different association of the PKCα C1A and C1B domains with PS lipids.

Even though transiently in our simulations the PKCα C1A domain can bind as many as 4−5 PS lipids while the PKCα C1B domain can bind as many as 2−3 PS lipids (Figure 4), the PS binding stoichiometry (time averaged) is only 1.2 ± 1.0 and 0.3 ± 0.6, respectively. The large uncertainties of those values highlight the dynamic nature of the C1 domain-PS association.

Subsequent to these MD studies, further evidence consistent with the higher positive charge and PS stoichiometry of the C1A domain relative to the C1B domain has been obtained experimentally by single molecule TIRF microscopy (SM-TIRFM) studies. Illustrated in Figure 5, these experiments have revealed that the membrane binding affinity of the C1A domain is much more sensitive to the PS density than the C1B domain. As expected, both proteins bind bilayers more efficiently (relative to pure PC bilayers) when PS lipids are present. Interestingly, our SM-TIRFM experiments found that the C1A domain has significantly higher affinity for PS-containing membranes than the C1B domain, a finding that follows the trend of their relative PS binding stoichiometry suggested by our MD simulations.

Closer examination of the PS binding events in our simulations shows that none of the identified interacting sites were persistently bound to PS (Figure 4). For example, each one of the residues R42, K45, K62, and K76 in the PKCα C1A domain was found associated with PS lipids for 26−30% of the time and with R77 for 17% of the time, while K105 and K141 in the C1B domain showed association with PS lipids for only about 10 and 18% of the time, respectively. These results indicate that the C1 domain-PS association is not saturated, and thus is not high affinity. However, as depicted by the snapshots from our simulations (Figure 4), at least some of the PS binding sites provide multiple headgroup contacts. Given the basic residues in the PKCα C1 domains, the PS enantiomer (1,2-*sn*-phosphatidyl-L-serine) appears to be highly suitable to bind more than one of the basic residues, presumably due to the two separated negatively charged centers as well as the stereochemistry. We estimate that 80−90% of the C1-PS multivalent contacts in our simulations are better enabled by the physiological enantiomer 1,2-*sn*-phosphatidyl-L-serine than by the nonphysiological enantiomer 2,3-*sn*-phosphatidyl-D-serine. This is consistent with the findings of Newton and co-workers, which show that the nonphysiological enantiomer 2,3-*sn*-phosphatidyl-D-serine exhibits significantly lower affinity for PKCs.[45] In addition, our simulations also provide structural evidence to support earlier experiments[45,46] which discovered that cPKC has higher affinity for PS than for other lipids (like

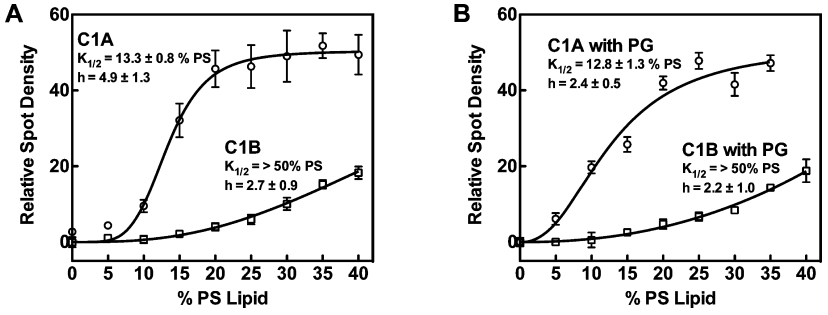

Figure 5. Dependence of C1A and C1B bilayer binding on phosphatidylserine (PS) density. Membrane density of proteins was quantified by SM-TIRFM as described previously.[29] C1A or C1B concentration was fixed at 5 pM and added to supported phosphatidylcholine (PC) bilayers containing (A) increasing amounts of PS lipid or (B) increasing amounts of PS lipid where total anionic lipid was kept at 40% using phosphatidylglycerol (PG) lipid. After a brief incubation to ensure steady state binding, the density of fluorescent, membrane bound proteins was measured for 5 temporally isolated frames from three separate movie streams in three separate titration experiments. In order to remove purely electrostatic binding due to PG lipid, the additional binding signal measured from 0 to 40% PS lipid was removed. The resulting binding is thus due to specific protein interactions with PS since nonspecific electrostatic recruitment has been removed.

dx.doi.org/10.1021/ja505369r | J. Am. Chem. Soc. 2014, 136, 11757−11766

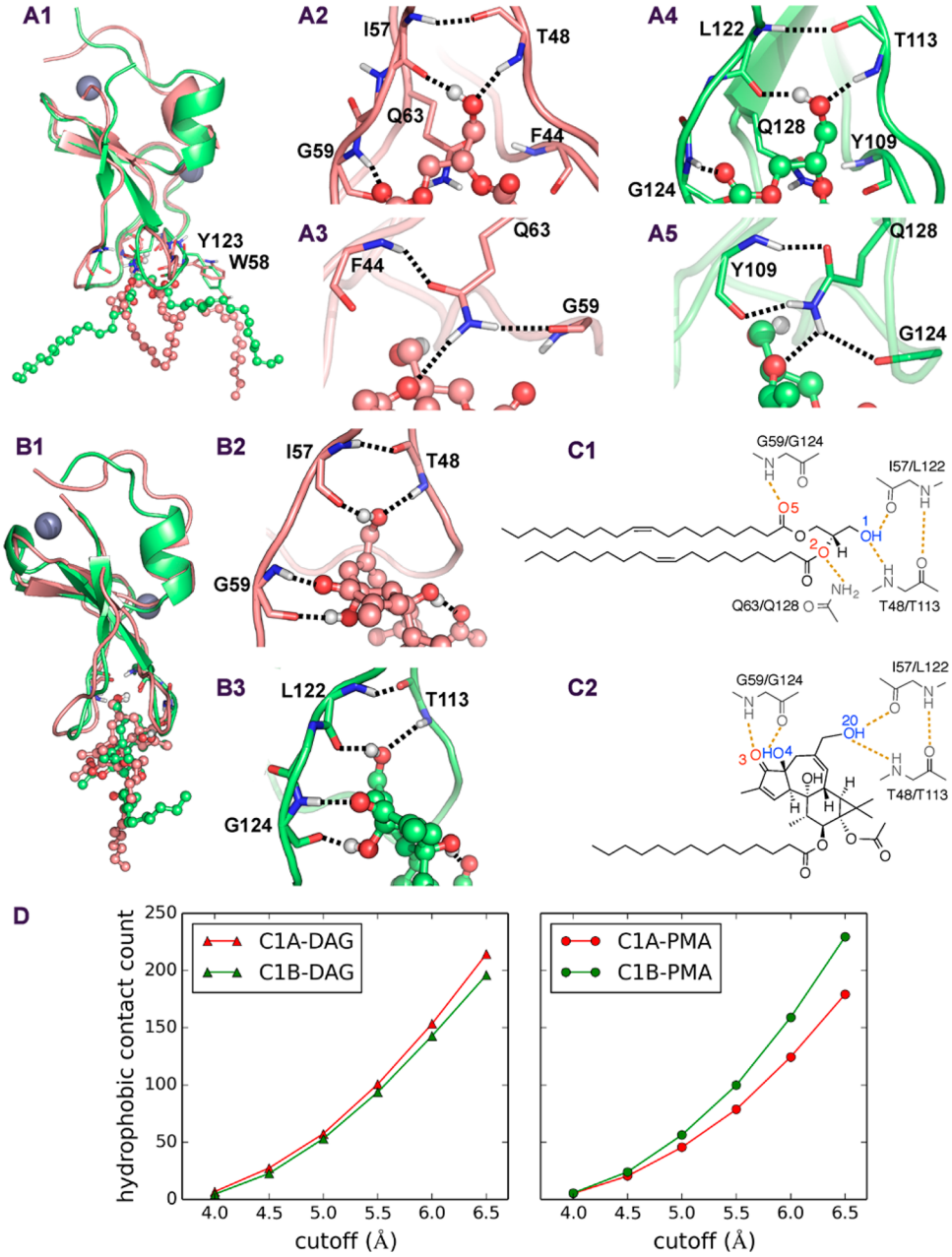

Figure 6. (A1) Structural representations of superimposed DAG-bound C1A and C1B conformations. The conformations were obtained from representatives of the most probable complex clusters. Cartoon illustrations of (A2,3) hydrogen bonds between DAG and the C1A domain, and (A4,5) hydrogen bonds between DAG and the C1B domain. (B1) Structural representations of superimposed PMA-bound C1A and C1B conformations. (B2,3) hydrogen bonds between PMA and the C1A and C1B domains. (C1,2) Illustration of the hydrogen bonds between the activators and the proteins. (D) Comparison of the nonpolar contacts.

PC, PA, and PE). Thus, although there is no high affinity PS-binding site observed in the PKCα C1 domains, the multivalent C1-PS interactions can explain the observed stereospecificity of C1 for the PS enantiomer.

Taken together, the findings of our MD simulations and SM-TIRFM experiments suggest a simple mechanism for the positive cooperativity observed in experimental C1 domain binding measurements when the bilayer PS density is varied and a fixed bilayer negative charge is maintained (Figure 5). In this model, the C1 domain first associates with the bilayer by interacting with a single PS molecule, then subsequently interacts with one or more additional PS molecules. In such a system, the initial PS association will increase the affinities of subsequent PS binding events, leading to positive cooperativity.

PKCα C1 Domains in the PC: PS Membrane with DAG/PMA Activators. To explore the detailed C1 domain-activator interactions, we simulated the activator-bound C1 complexes in the PC:PS membrane with additional unbound activators. In the absence of structural information for ligand-bound PKCα C1 domains, we tested different activator-bound poses and obtained only one pose for each complex that is stable for the entire 300 ns membrane-bound simulation, with the protein Cα RMSD mainly fluctuating between 1.0 to 2.6 Å. Compared to the activator-free cases, DAG binding induced 1.8 and 1.6 Å decreases on average in the loop-tip distance for C1A and C1B

dx.doi.org/10.1021/ja505369r | J. Am. Chem. Soc. 2014, 136, 11757−11766

respectively, while PMA binding induced 3.0 and 0.5 Å decreases, respectively, with all ligand-bound states yielding much narrower distributions (see Figure S1 (SI)). These observations suggest that activator binding leads to closing of the groove and a higher degree of protein rigidity.

The association of PS with the PKCα C1 domains is not altered significantly in our simulations by the presence of lipid activators. It is estimated that the average number of bound PS lipids for the C1A and C1B domains are 1.0 ± 1.0 and 0.2 ± 0.4 with DAG and 0.9 ± 1.0 and 0.4 ± 0.6 with PMA, suggesting that the interaction of the C1 domains with PS is still highly dynamic. Major sites of PS interaction are identical to the activator-free cases: R42, K45, K62, K76 and R77 in the C1A domain and K105 and K141 in the C1B domain. These results again support the notion that binding of the C1 domains to lipid activators has little direct impact on their association with PS lipids.

In order to further examine why the PKCα C1A and C1B domains might have opposite affinities to bind DAG and PMA,[33] we compared the hydrogen bonds and nonpolar contacts in all four complexes. Surprisingly, a highly conserved hydrogen-bonding pattern is observed, although this pattern does not appear sufficient to account for the different activating lipid preferences of the two domains. The backbone of conserved residues, including T48, I57, and G59 of the C1A domain and T113, L122, and G124 of the C1B domain, form consistent hydrogen bonds with DAG and PMA (Figure 6). The 1-hydroxyl of DAG or the 20-hydroxyl of PMA, serving as both a donor and an acceptor of hydrogen bonds, connects backbone atoms of I57 and T48 in the C1A domain or L122 and T113 in the C1B domain (Figure 6C1,C2). The I57/L22 backbone NH donates a hydrogen bond to the T48/T113 backbone carbonyl, so that the β12 and β34 loops are bridged (Figure 6C1,C2). This hydrogen-bonding triangle likely determines the activator orientation in the binding groove. Additionally DAG and PMA also form hydrogen bonds with backbone atoms of G59 and G124 to further anchor the complex conformations. In the absence of water, this hydrogen-bonding network plays a key role for activators to access the binding groove, as well as to stabilize the C1 domains in their membrane-bound states. It is noteworthy that the Raf-1 C1 domain,[47] an atypical C1 domain lacking binding to DAG, is incapable of forming these hydrogen bonds due to a much shorter β34 loop (see Figure S2 (SI)), which highlights the importance of these specific hydrogen bonds.

While the hydrogen-bonding network involving the protein backbone seems to be conserved among the PKCα C1 and the PKCδ C1B domains,[11] the side-chain polar contacts appear as an obvious difference between DAG and PMA. In our simulations, the side chains of Q63 of the C1A domain and Q128 of the C1B domains are hydrogen bonded to not only the backbone of both β12 and β34 loops but also with DAG (Figure 6A3,A5). No such contact is observed, however, between Q63/Q128 and PMA, since in this case the glutamine side chain is less stretched and cannot reach to provide the contacts. Our results show further, general evidence to support an earlier finding regarding Q128 of the PKCα C1B domain,[37] which suggests that this conserved glutamine residue plays a key role to modulate the shape and the contacts of the activator-binding groove.

While the conserved hydrogen-bonding network still does not explain the opposite activator lipid preference of the PKCα C1A and C1B domains, our analysis of nonpolar contacts does provide a plausible explanation of this disparity. In Figure 6D, the number of nonpolar contacts between the activators and the C1 domains are plotted against increasing cutoffs in the definition of the contact distances. DAG always has more nonpolar contacts with the C1A domain than with the C1B domain, regardless of the cutoffs employed. The opposite behavior is observed for PMA, which always has more nonpolar contacts with the C1B domain. When changing from DAG to PMA, the number of nonpolar contacts decreases for C1A but increases for C1B. Estimates of the PISA interfacial energies[48] show that the C1A-DAG complex is more stable than the C1A-PMA complex by 2.1 kcal/mol, while the C1B-PMA complex more stable than the C1B-DAG complex only by 0.8 kcal/mol. These results therefore provide semiqualitative evidence for the binding preferences of C1 domains.[33] Moreover, our simulations are also able to identify the most relevant residues (with over 2 activator contacts on average), which include F43, P47, W58, F60, and L63 in the C1A domain when bound to DAG, and P112, Y123, L125, Q128 in the C1B domain when bound to PMA. These findings are in agreement with prior mutagenesis experiments,[35] which showed that some of these residues (in particular W58 and F60) are essential for DAG activator binding.

In addition to DAG/PMA interactions, we also monitor the unbound ligands in each simulation (see Figure S3 (SI)). Even though the unbound DAG or PMA molecules are close enough to the C1 domain in our starting conformations, they do not dwell near the proteins. At the end of the 300 ns simulations, all unbound DAG and PMA ligands move away from the protein, exhibiting a separation of over 10 Å from the closest protein heavy atom. In line with previous experimental observations,[12] our simulations does not show a secondary site in the C1 domains for DAG or PMA binding, suggesting a binding stoichiometry of 1:1 for activators binding to each PKCα C1 domain.

Motion of the PKCα C1 Domains in Membranes. We did not observe obvious tilting of the membrane-bound PKCα C1 domains in simulations, as demonstrated by the small values and narrow distributions of the angles between the longest protein principal axis and the Z-axis. These angles are 17 ± 8 for the C1A domain and 16 ± 8 degrees for the C1B domain in the PC:PS membrane, while they reach values of 16 ± 8 for the C1A domain and 12 ± 7 degrees for the C1B domain in PC:PS +DAG membrane as well as 14 ± 8 (C1A) and 13 ± 9 (C1B) degrees in PC:PS+PMA. These results show a consistent orientation of the PKCα C1 domains inserted in membranes and confirm once more the overall stability of the models employed in our simulations.

Furthermore, we examined the membrane penetration of the PKCα C1 domains. Our simulations show that these two domains are not fixed in the membranes. Defined as the distance from the domain center of mass to the N-plane of DOPC, the membrane insertion depth of the C1A and C1B domains can vary continuously from the deep state (∼−2 Å) to the shallow state (∼10 Å), with the distributions shown in Figure S4 (SI). In the deep state the hydrophobic half of the C1 domains is embedded in the membrane, while in the shallow state the tips of the loops barely touch the membrane. These results confirm, at the molecular level, the two states of the membrane-bound PKCα C1 domains identified in our earlier experiments,[29] although the MD simulations may not be long enough to fully define the ratio of time spent in the deep and shallow states. The average membrane insertion depth is 3.9−

4.0 Å for all our constructs except for the PMA-bound C1B domain, which has a mean value of 4.4 Å (see Figure S4 (SI)). It is suggested that DAG or PMA binding does not generally modify membrane penetration for the C1 domains except that PMA induces the C1B domain to move to more shallow positions.

In addition to the orientation and membrane penetration, we have also measured protein diffusion coefficients via simulations as well as by experiments. While such calculations in membranes are very difficult to converge and their results should be viewed with caution, we note that our atomistic simulations compare reasonably well to earlier coarse-grained ones of membrane proteins in free-standing lipid bilayers.[15,49] Although the absolute diffusion coefficients from our atomistic simulations are about 1 order of magnitude larger than the experimental values, we achieve qualitative agreement between simulations and experiments (Table 1). In spite of the different membrane constructs (simulations with free-standing bilayers versus experiments with supported bilayers), both simulations and experiments agree that the PKCα C1 domains have very similar diffusion coefficients (D_L) in membranes with and without activators, except that the PMA-bound C1B domain has a much higher D_L than other assemblies. As suggested in prior work,[12,29] membrane penetration is an important determinant of membrane protein peripheral diffusion. It is likely that the shallow insertion depths of the PMA-bound C1B domain observed in our simulations is related to the increased diffusion coefficient measured in both simulations and experiments. A unique finding from simulations for the PMA-C1B complex is that its membrane insertion depth becomes shallower by about 2.8 Å from 150 to 300 ns. In fact, the fraction of the conformations with insertion depth shallower than 4.4 Å increases for ∼20% every 50 ns only for the PMA-bound C1B domain, while no obvious increase is observed for other constructs. Additionally, unique to the PMA-bound C1B domain, the activator tail-to-tail contacts to the PC or PS lipids decrease for 50% from ∼200 to 300 ns in our long simulation. We therefore hypothesize that the joint effect of weak interactions with the PS head groups and reduced contacts to the membrane hydrophobic core results in a higher occurrence of the shallow state, which could be responsible for the comparatively fast diffusion of the PMA-bound C1B domain. The relatively larger effect of PMA on the experimental diffusion coefficient of C1B may arise from the longer time scale and spatial dimension of the diffusion measurement.

Table 1. Peripheral Diffusion Coefficients D_L Obtained from MD Simulations with Free-Standing Bilayers and Experiments with Supported Bilayers (Units: $\mu m^2/s$)[a]

	PKCα C1A		PKCα C1B	
	simulations	experiments	simulations	experiments
PC:PS	12.8 ± 1.8	0.7 ± 0.1	15.1 ± 1.4	0.5 ± 0.1
PC:PS+DAG	14.6 ± 2.2	0.7 ± 0.1	15.6 ± 2.1	0.6 ± 0.2
PC:PS+PMA	12.3 ± 1.8	0.7 ± 0.1	20.3 ± 3.0	1.2 ± 0.1

[a]Error bars of simulation data were calculated from 2 trajectories of the same construct. Error bars of experimental data were calculated from 5 experiments of the same construct, each containing at least 300 trajectories.

Detailed Membrane Interaction Mechanism of the PKCα C1 Domains. Connecting the evidence from our systematic combined study, we propose the possible detailed membrane-binding mechanism of the PKCα C1 domains. Compared to the PKCα C2 domain, which has been studied in our previous work,[43] we found that the interactions of PS with C1 are weaker than with C2. In line with the previously proposed activation mechanism,[29] the C2 domain rather than either C1 domains is likely to direct PKCα to the membrane. For the subsequent activation steps, although the solvent exposure of these two C1 domains in the full-length PKC might differ, our study supports the notion that the C1A domain is recruited to the membrane before the C1B domain due to its much stronger interactions with anionic PS lipids. Once it is bound to the membrane, the C1A or C1B domain likely undergoes conformational changes to open the activator-binding groove, while at the same time the entire domain fluctuates between the shallow and deep states of membrane insertion. Deep membrane insertion enhances the stability of the open groove conformations, which may relate to the searching mechanism for activators. When a PKCα C1 domain binds an activator, the activator-binding groove likely becomes closed, and the entire domain turns more rigid. The conserved hydrogen bonds are important for activator recognition and binding orientation in the membrane-bound environment. However, it is the nonpolar contacts between the C1 domains and the activators that lead to the opposite activator-binding preference. Finally, PMA binding appears to favor the shallow binding state of the C1B domain, as observed in the MD simulations and suggested by experimental diffusion coefficients. The findings of strong nonpolar contacts between PKCα C1B and PMA, reduced contacts between the membrane and the C1B-PMA complex, and abnormally fast diffusion of the PMA-bound C1B domain may be relevant to the molecular mechanism of tumor promotion induced by PMA and other phorbol esters.

■ CONCLUSIONS

We have combined modeling, simulations, and experiments to study the C1A and C1B domains of PKCα in membranes, a difficult task with a single approach alone. Our findings of previous[12,29,43] and current work suggest the following detailed mechanism involving the C1A and C1B domains during PKCα activation: After the entire PKCα is associated with the membrane, both C1 domains can bind to the membrane during activation. The C1A domain is recruited first with strong interactions to lipid coactivator PS and activator DAG, and the C1B domain is recruited later with a preference to bind activator PMA. The two PKCα C1 domains are encoded in their sequences to play different roles, via the distinct surface electrostatic contacts with coactivors as well as nonpolar contacts with activators. Our study has provided evidence to support the notion that C1B binding to the membrane by activating lipids could likely be the key step in the PKCα activation model.

In addition, corroborating evidence is obtained from simulations and experiments in terms of lipid binding and protein diffusion. Simulations and experiments complement each other and enable us to connect evidence in multiple spatial and temporal scales of the C1 domains interacting with membranes. Our combined approach will be useful in exploring the roles of the C1 domains in many signaling proteins, even in the absence of detailed structural information, and help to further understand their molecular mechanisms in normal cellular function and disease development. Given the approach of atomistic MD simulations used here, it is important to be

aware of the difference between our simulations and experiments in time and length scales. Future efforts will be to develop accurate coarse-grained lipid and protein models to better explain and predict protein dynamics on experimental time scales. In order to gain further information on PKCα activation, we are also simulating a full-length model with the knowledge gained from the individual domains in our PKCα studies[12,29,43] as well as from this work.

MATERIALS AND METHODS

Membrane-Bound Model Construction. We have modeled and simulated the individual C1A and C1B domains in membranes and buffers that mimic the experimental conditions. In many experiments, an engineered C1 domain is fused with a ~300-residue maltose-binding protein (MBP), which serves to enhance the solubility of the C1 domains.[29] As shown in the Supporting Information, we confirmed that both the MBP and the peptide linkers have negligible impact on the interactions between the C1 domains and membranes (see Figure S5 (SI)). It is, therefore, reasonable to only model individual C1 domains in order to understand the detailed protein−lipid interactions.

At the beginning, the membrane models and protein models were built independently. The 3:1 PC:PS symmetric bilayer model, containing 120 DOPC and 40 DOPS lipids, was set up with the CHARMM-GUI membrane builder[50] and pre-equilibrated in a water box (containing 150 mM NaCl solution) for 20 ns using the CHARMM36 force field and the Desmond 3.0 simulation package.[51] The membrane model was then aligned to the $X-Y$ plane, perpendicular to the Z-axis. The PKCα C1B model (residue 102−151) was based on the coordinates of the solution structure from residue 18−67 (PDB code: 2ELI). The PKCα C1A model (residue 37−86, Figure 1) was generated by the homology-modeling server SWISS-MODEL,[52] with 42% sequence identity to the template (PDB code: 1PTR). To examine the protonation states of the ionic residues, the Protein Preparation Wizard implemented in Maestro (version 9.3, Schrödinger, LLC, 2012) was used. Each Zn^{2+} ion was ligated by three cysteine residues in the thiolate form and one histidine residue singly protonated on the δ-nitrogen atom in our starting protein conformations.

The PKCα C1A and C1B models were then combined with the PC:PS membrane. Each C1A or C1B structure was aligned, rotated, and moved below the membrane model, so that the long axes of the protein was almost parallel to the Z-axis and the tip of the β12 and β34 loops could point toward the lower leaflets of the membranes. As suggested by preliminary experimental data,[12,29] the protein center was set 6 Å below the N-plane of DOPC in the lower leaflet to insert the protein model into the membrane model. Almost half of the C1A/C1B domain was in the lower leaflet, but did not reach the upper leaflet. With System Builder in Maestro, a water box containing 140 mM NaCl and 10 mM KCl was created in each construct, whose boundary was at least 15 Å from the closest protein or lipid atoms in the Z direction. Since trapping water between a C1 domain and the membrane is generally unfavorable,[11] water molecules were excluded near the protein−membrane interface.

DAG and PMA molecules were inserted to the membrane, in order to model the C1 domains in the presence of activators. The PMA-bound models were built according to alignment of the ligand-bound PKCδ C1B structure (PDB code: 1PTR) to the protein structure in the above-mentioned models, followed by modification of the phorbol ester ligand to PMA. Since DAG has been found to compete with PMA for the same binding site,[53] we aligned selected oxygen atoms of DAG to the ones of the phorbol compound in the crystal structure, and thus several DAG-bound C1A and C1B constructs were built and tested in our search for stable complexes. In addition to the bound activator, two DAG or PMA molecules were inserted adjacent to the proteins to examine any secondary binding or interacting sites.

In short, three membrane compositions (PC:PS, PC:PS+DAG, and PC:PS+PMA) for the PKCα C1A and C1B domains were used to build 6 constructs. Each construct contains about 52 000 atoms in a ~85 Å × 85 Å × 85 Å box with periodic boundary conditions.

Atomistic MD Simulations. We applied the tool Viparr in Desmond to assign all-atom force field parameters. The protein parameters were obtained from the CHARMM27 cmap force field, except that the thiolate parameters were adopted from a prior report.[54] The CHARMM36 parameters were used for DOPC and DOPS, and the CHARMM General Force Field for DAG and PMA.[55] The TIP3P model was used for explicit water molecules. After parameter assignment, the starting models were minimized to remove steric clashes and relaxed with the standard protocol in the Maestro-Desmond package. We used a script in the package with the M-SHAKE algorithm to constrain the bond length of all bonds involving hydrogen atoms, as well as the angle in all water molecules. Our production simulations were conducted with Desmond 3.0 with a 2 fs time step. The bonded and near interactions were updated every step, while the far interactions were updated every three steps. These semi-isotopic simulations were performed at constant temperature (296 K) and constant pressure (1 bar). The Nosé−Hoover Chain thermostat method was employed together with the Martyna−Tobias−Klein barostat. The short-range cutoff to calculate Coulombic and Lennard−Jones interactions was 9.0 Å. The long-range Coulombic interactions were treated with the smooth particle mesh Ewald method. Two replica simulations were run for each construct: a short one for 150 ns and a long one for 300 ns. Consistence of our short and long simulations suggests that our simulation time scale is sufficient to remove starting conformation bias.

Simulation Data Analyses. Conformational analyses were performed with VMD[56] and Pymol (Schrödinger, LLC). In this work, root-mean-square deviations (RMSDs) of protein conformations were computed on C_α atom pairs with alignment to the reference PKCα C1B structure (residue 18−67, PDB code: 2ELI). A salt bridge or a charged contact is defined when two polar atoms with opposite charges are within 4.0 Å. Bound lipids are defined as those which have heavy atoms within 4.0 Å of the closest protein heavy atom with the opposite charge. A hydrophobic contact is defined when two nonpolar atoms (partial charge <0.3 unit) are within the cutoff distance. The protein orientation in the membrane is measured as the angle between the protein's longest principal axis and the Z-axis.

The peripheral diffusion coefficient (D_L) of the PKCα C1 domains was calculated from the mean-square displacement (MSD) over time according to eq 1:

$$D_L = \lim_{t\to\infty} \frac{\mathrm{MSD}(t)}{4t} = \lim_{t\to\infty} \frac{\langle |\mathbf{r}(t+t_0) - \mathbf{r}(t_0)|^2 \rangle}{4t} \quad (1)$$

where $\mathbf{r}$ is the center of mass vector of the C1A or C1B domain. The averaging was calculated over the blocks in the divided simulations. The overall drift of the lower leaflet was removed from the protein diffusion,[57] and only the second half of each trajectory was used during our MSD calculation. Plots of MSD versus time are shown in Figure S6 (SI).

The angle between the longest protein principal axis and the Z-axis was measured to examine the protein orientation in membranes. To quantify membrane penetration, the membrane insertion depth of the PKCα C1 domains was defined as the distance from the protein's center of mass to the closest nitrogen plane of the DOPC lipids.

Experiments. Reagents and experimental protocols are consistent with previously described work[12,15,29] and will be described briefly.

Bacterial expression constructs of human PKCα C1A and C1B regulatory domains were constructed by inserting DNA sequences encoding C1A domain (residues 26−100) and C1B domain (90−165) into a pMAL-c2G expression vector. For each protein, primers were designed to incorporate an N-terminal 11-amino acid recognition sequence for Sfp phospho-pantethienyl-transferase to enable sequence-specific enzymatic labeling with a CoA-linked fluorophore.

The C1A and C1B domains were expressed in *Escherichia coli* Rosetta 2(DE3) cells (Novagen). Overnight expression at 20 °C was followed by purification on amylose resin (NEB) and eluted with excess maltose. Purified proteins were ≥90% of total eluted protein.

The N-terminal Sfp labeling tag was covalently modified with an Alexa Fluor 555-CoA by the Sfp enzyme, and excess fluorophore was removed using Vivaspin concentrators (Sartorius Stedim, Göttingen, Germany).

To generate supported bilayers, sonicated unilammelar vesicles (SUVs) comprised of synthetic dioleolyl phospholipids PC (phosphatidylcholine; 1,2-dioleoyl-*sn*-glycero-3-phosphocholine), PS (phosphatidylserine; 1,2-dioleoyl-*sn*-glycero-3-phospho-L-serine), DAG (diacylglycerol; 1,2-dioleoyl-*sn*-glycerol), PG (1,2-dioleoyl-*sn*-glycero-3-phospho-(1′-*rac*-glycerol)) [all from Avanti Polar Lipids (Alabaster, AL)] and PMA (phorbol-12-myristate-13-acetate) [from Sigma-Aldrich (St. Louis, MO)] were deposited onto piranha-cleaned glass substrates.

TIRF microscopy measurements were carried out at 22 °C ± 0.5 °C on a home-built, objective-based instrument as previously described.[12,15,29] Supported bilayers were imaged before and after the addition of physiological buffer (140 mM KCl, 15 mM NaCl, 0.5 mM MgCl, 26 μM $CaCl_2$, 20 μM EGTA, 5 mM reduced L-glutathione, 25 mM HEPES, pH 7.4) and a blocking step with BSA in order to account for fluorescent contaminants, which typically were few. After a 5 min incubation with protein, samples were bleached at high laser powers to minimize contributions from immobile fluorescent particles followed by a 60 s recovery. For each sample, multiple movie streams were acquired at a frame rate of 20 frames/s and a spatial resolution of 4.2 pixels/μm. Particle tracking analysis and fitting were carried out using ImageJ, GraphPad Prism 5 and Mathematica.

■ ASSOCIATED CONTENT

Supporting Information

Distributions of loop-tip distance measured with atomistic MD simulations (Figure S1), superimposed structures of atypical C1 domain and DAG-bound models of PKCα C1 domains (Figure S2), lateral diffusion paths of unbound activators (Figure S3), comparisons of membrane insertion depths (Figure S4), and analysis and final snapshot of MBP-C1A-C1B simulations (Figure S5). Mean-square displacement versus time plots (Figure S6). This material is available free of charge via the Internet at http://pubs.acs.org.

■ AUTHOR INFORMATION

Corresponding Author

gavoth@uchicago.edu

Notes

The authors declare no competing financial interest.

■ ACKNOWLEDGMENTS

This research is supported by National Institutes of Health Grants R01 GM-063796 (to G.A.V.) and R01 GM-063235 (to J.J.F.). This work used the Extreme Science and Engineering Discovery Environment (XSEDE), which is supported by National Science Foundation Grant Number OCI-1053575. Computational resources were provided by XSEDE Kraken and the Research Computing Center (RCC) at the University of Chicago. We thank Drs. Anand Srivastava and Severin T. Schneebeli for helpful discussion.

■ REFERENCES

(1) Hurley, J. H.; Misra, S. *Annu. Rev. Biophys. Biomol. Struct.* **2000**, *29*, 49.
(2) Hurley, J. H. *Biochim. Biophys. Acta, Mol. Cell Biol. Lipids* **2006**, *1761*, 805.
(3) Cho, W.; Stahelin, R. V. In *Protein–Lipid Interactions*; Wiley-VCH Verlag GmbH & Co. KGaA: Weinheim, 2006; p 367.
(4) Hurley, J. H.; Newton, A. C.; Parker, P. J.; Blumberg, P. M.; Nishizuka, Y. *Protein Sci.* **1997**, *6*, 477.
(5) Mellor, H.; Parker, P. J. *Biochem. J.* **1998**, *332*, 281.
(6) Cho, W. H.; Stahelin, R. V. *Annu. Rev. Biophys. Biomol. Struct.* **2005**, *34*, 119.
(7) Rosse, C.; Linch, M.; Kermorgant, S.; Cameron, A. J.; Boeckeler, K.; Parker, P. J. *Nat. Rev. Mol. Cell Biol.* **2010**, *11*, 103.
(8) Baldanzi, G. *Adv. Biol. Regul.* **2014**, *55*, 39.
(9) Steinberg, S. F. *Physiol. Rev.* **2008**, *88*, 1341.
(10) Colon-Gonzalez, F.; Kazanietz, M. G. *Biochim. Biophys. Acta* **2006**, *1761*, 827.
(11) Zhang, G. G.; Kazanietz, M. G.; Blumberg, P. M.; Hurley, J. H. *Cell* **1995**, *81*, 917.
(12) Ziemba, B. P.; Falke, J. J. *Chem. Phys. Lipids* **2013**, *172–173*, 67.
(13) Slater, S. J.; Ho, C.; Kelly, M. B.; Larkin, J. D.; Taddeo, F. J.; Yeager, M. D.; Stubbs, C. D. *J. Biol. Chem.* **1996**, *271*, 4627.
(14) Shindo, M.; Irie, K.; Nakahara, A.; Ohigashi, H.; Konishi, H.; Kikkawa, U.; Fukuda, H.; Wender, P. A. *Bioorg. Med. Chem.* **2001**, *9*, 2073.
(15) Knight, J. D.; Lerner, M. G.; Marcano-Velazquez, J. G.; Pastor, R. W.; Falke, J. J. *Biophys. J.* **2010**, *99*, 2879.
(16) Konopatskaya, O.; Poole, A. W. *Trends Pharmacol. Sci.* **2010**, *31*, 8.
(17) Mochly-Rosen, D.; Das, K.; Grimes, K. V. *Nat. Rev. Drug Discovery* **2012**, *11*, 937.
(18) Griner, E. M.; Kazanietz, M. G. *Nat. Rev. Cancer* **2007**, *7*, 281.
(19) Kim, J.; Thorne, S. H.; Sun, L.; Huang, B.; Mochly-Rosen, D. *Oncogene* **2011**, *30*, 323.
(20) Molkentin, J. *Circulation* **2008**, *118*, A18.
(21) Liu, Q. H.; Molkentin, J. D. *J. Mol. Cell. Cardiol.* **2011**, *51*, 474.
(22) Geraldes, P.; King, G. L. *Circ. Res.* **2010**, *106*, 1319.
(23) Kellerer, M.; Mushack, J.; Seffer, E.; Mischak, H.; Ullrich, A.; Haring, H. U. *Diabetologia* **1998**, *41*, 833.
(24) Zarate, C. A.; Manji, H. K. *CNS Drugs* **2009**, *23*, 569.
(25) Manji, H. K.; Lenox, R. H. *J. Clin. Psychiatry* **2000**, *61*, 42.
(26) Burns, D. J.; Bell, R. M. *J. Biol. Chem.* **1991**, *266*, 18330.
(27) Newton, A. C. *J. Biol. Chem.* **1995**, *270*, 28495.
(28) Leonard, T. A.; Rozycki, B.; Saidi, L. F.; Hummer, G.; Hurley, J. H. *Cell* **2011**, *144*, 55.
(29) Ziemba, B. P.; Li, J.; Landgraf, K. E.; Knight, J. D.; Voth, G. A.; Falke, J. J. *Biochemistry* **2014**, *53*, 1697.
(30) Scott, A. M.; Antal, C. E.; Newton, A. C. *J. Biol. Chem.* **2013**, *288*, 16905.
(31) Pérez-Lara, Á.; Egea-Jiménez, A. L.; Ausili, A.; Corbalán-García, S.; Gómez-Fernández, J. C. *Biochim. Biophys. Acta, Mol. Cell Biol. Lipids* **2012**, *1821*, 1434.
(32) Giorgione, J.; Hysell, M.; Harvey, D. F.; Newton, A. C. *Biochemistry* **2003**, *42*, 11194.
(33) Ananthanarayanan, B.; Stahelin, R. V.; Digman, M. A.; Cho, W. *J. Biol. Chem.* **2003**, *278*, 46886.
(34) Dries, D. R.; Gallegos, L. L.; Newton, A. C. *J. Biol. Chem.* **2007**, *282*, 826.
(35) Medkova, M.; Cho, W. H. *J. Biol. Chem.* **1999**, *274*, 19852.
(36) Bittova, L.; Stahelin, R. V.; Cho, W. *J. Biol. Chem.* **2001**, *276*, 4218.
(37) Stewart, M. D.; Morgan, B.; Massi, F.; Igumenova, T. I. *J. Mol. Biol.* **2011**, *408*, 949.
(38) Antal, C. E.; Violin, J. D.; Kunkel, M. T.; Skovso, S.; Newton, A. C. *Chem. Biol.* **2014**, *21*, 459.
(39) Kimura, K.; Mizutani, M. Y.; Tomioka, N.; Endo, Y.; Shudo, K.; Itai, A. *Chem. Pharm. Bull.* **1999**, *47*, 1134.
(40) Pak, Y.; Enyedy, I. J.; Varady, J.; Kung, J. W.; Lorenzo, P. S.; Blumberg, P. M.; Wang, S. M. *J. Med. Chem.* **2001**, *44*, 1690.
(41) Kang, J. H.; Benzaria, S.; Sigano, D. M.; Lewin, N. E.; Pu, Y. M.; Peach, M. L.; Blumberg, P. M.; Marquez, V. E. *J. Med. Chem.* **2006**, *49*, 3185.
(42) Hritz, J.; Ulicny, J.; Laaksonen, A.; Jancura, D.; Miskovsky, P. *J. Med. Chem.* **2004**, *47*, 6547.
(43) Lai, C.-L.; Landgraf, K. E.; Voth, G. A.; Falke, J. J. *J. Mol. Biol.* **2010**, *402*, 301.
(44) Newton, A. C.; Keranen, L. M. *Biochemistry* **1994**, *33*, 6651.

(45) Johnson, J. E.; Zimmerman, M. L.; Daleke, D. L.; Newton, A. C. *Biochemistry* **1998**, *37*, 12020.
(46) Johnson, J. E.; Giorgione, J.; Newton, A. C. *Biochemistry* **2000**, *39*, 11360.
(47) Mott, H. R.; Carpenter, J. W.; Zhong, S.; Ghosh, S.; Bell, R. M.; Campbell, S. L. *Proc. Natl. Acad. Sci. U. S. A.* **1996**, *93*, 8312.
(48) Krissinel, E.; Henrick, K. *J. Mol. Biol.* **2007**, *372*, 774.
(49) Goose, J. E.; Sansom, M. S. P. *PLoS Comput. Biol.* **2013**, *9*, e1003033.
(50) Jo, S.; Lim, J. B.; Klauda, J. B.; Im, W. *Biophys. J.* **2009**, *97*, 50.
(51) Bowers, K. J.; Chow, E.; Xu, H.; Dror, R. O.; Eastwood, M. P.; Gregersen, B. A.; Klepeis, J. L.; Kolossvary, I.; Moraes, M. A.; Sacerdoti, F. D.; Salmon, J. K.; Shan, Y.; Shaw, D. E. In *Proceedings of the 2006 ACM/IEEE Conference on Supercomputing*; ACM: Tampa, FL, 2006; p 84.
(52) Arnold, K.; Bordoli, L.; Kopp, J.; Schwede, T. *Bioinformatics* **2006**, *22*, 195.
(53) Sharkey, N. A.; Leach, K. L.; Blumberg, P. M. *Proc. Natl. Acad. Sci. U. S. A.* **1984**, *81*, 607.
(54) Foloppe, N.; Sagemark, J.; Nordstrand, K.; Berndt, K. D.; Nilsson, L. *J. Mol. Biol.* **2001**, *310*, 449.
(55) Vanommeslaeghe, K.; Hatcher, E.; Acharya, C.; Kundu, S.; Zhong, S.; Shim, J.; Darian, E.; Guvench, O.; Lopes, P.; Vorobyov, I.; MacKerell, A. D. *J. Comput. Chem.* **2010**, *31*, 671.
(56) Humphrey, W.; Dalke, A.; Schulten, K. *J. Mol. Graphics Modell.* **1996**, *14*, 33.
(57) Klauda, J. B.; Brooks, B. R.; Pastor, R. W. *J. Chem. Phys.* **2006**, *125*, 144710.